**Sławomir KRAJEWSKI, Jerzy NOWACKI**

West Pomeranian University of Technology, Szczecin

doi:10.15199/48.2016.06.19

# Artificial Intelligence in the AHSS Steel Mechanical Properties and Microstructure Analysis

***Abstract***. *The assessment of results method of calculation tensile strength and yield strength of this cold rolled steels using the artificial neural networks in modelling relationship of elements composition (chromium, manganese, silicon, carbon), thermal treatment and properties of HCT600X, HCT780X, HCT980X steels was proposed. Was made further research using the new element chromium.*

***Streszczenie.*** *W artykule użyto sztucznych sieci neuronowych do obliczenia zależności między wytrzymałością na rozciąganie i umowną granicą plastyczności, a pierwiastkami (chrom, mangan, krzem i węgiel), obróbką cieplną i właściwościami stali HCT600X, HCT780X, HCT980X walcowanych na zimno należących do stali karoseryjnych dwufazowych. Dokonano kontynuację badań z uwzględnieniem nowego pierwiastka-chromu.* ***(Analiza właściwości mechanicznych stali karoseryjnych o wysokiej wytrzymałości z wykorzystaniem narzędzi sztucznej inteligencji)***

**Słowa kluczowe:** Sztuczna inteligencja w nauce o materiałach, Stale karoseryjne o wysokiej wytrzymałości, modelowanie mikrostruktury, modelowanie właściwości

**Keywords:** Artificial intelligence in materials science, Advanced High-Strength Steels, microstructure modeling, properties modelling.

## Introduction

Distinctive mechanical properties of Advanced High-Strength Steels (AHSS) result from phase transitions of coexistence temperatures of ferrite and super-cooled austenite in plastic strain conditions or rapid cooling from austenite in order to produce martensitic structure. AHSS became particularly advantageous to automotive industry due to their high tensile strength (up to 1700 MPa), high yield point (up to 1450 MPa), and high elongation A5 (up to 30%).

Car body sheets made with AHSS display better mechanical properties than those made of regular steels and allow for the reduction of the thickness of the construction, its mass as well as the energy needed for its production.

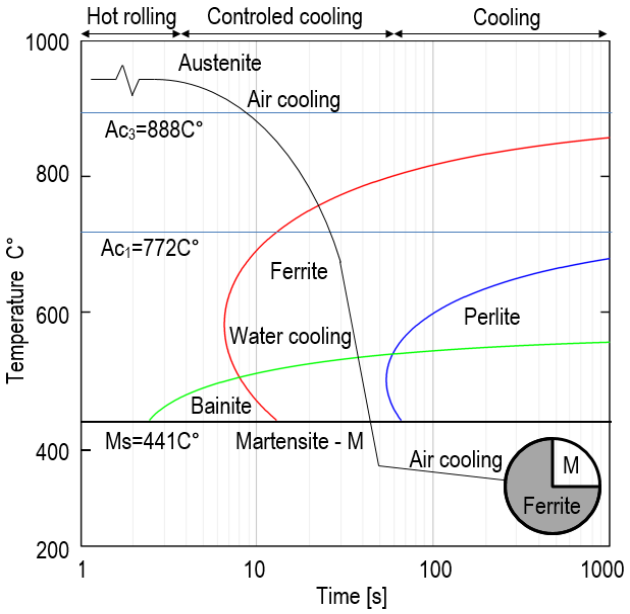


Fig. 1 Diagram of phase transformations during the cooling of dualphase steels.

Some of the major advantages of AHSS include their moderate price that results from a low number of alloy additions, reduction of construction thickness as well as favourable technological properties, including weldability and machinability. AHSS owe their fine mechanical properties to the multiphase structure of ferrite, bainite, martensite and retained austenite (Fig. 1).

Multiphase AHSS remain plastic despite martensite and/or bainite content. The process of steel working includes plastic strain being the result of hot or cold rolling (in case of Complex-phase steel) in austenite stability temperature (850°C) or cold rolling (in case of Dual-phase steel) called DP steels and rolling with controlled cooling [3÷7, 10].

The object of the present study is modelling the microstructure and properties of Dual-Phase Steels belonging to the grade of AHSS.

## Dual-phase steels microstructure

The steels selected for the purpose of the present study were dual phase steels in as supplied condition for the sake of their unique metastable residual austenite microstructure, consisting of 10÷50% of martensite in a fine-grain spheriodal ferrite matrix and 1-5% of, which determines their tensile strength (up to 1180 MPa) with unit elongation A5 up to 27%. The microstructure of DP steel is the effect of heat treatment (Fig. 1).

Among the steels used and presented in the study were steels produced by SSAB: HCT600X, HCT780X and HCT980X. Their chemical composition was determined with the use of the spectrometer LECO GDS 500A (see Table 1). The description of the steels examined was done on the basis of the observation of metallographic specimens etching in Nital 5% on the scanning electron microscope JOEL JSM-6100 (Fig. 2).

The relative volume of the phases in the microstructure of the steels examined was determined by means of computer image analysis in the NIS Elements 3.1 system (Table 3). X-ray structural analysis was done with the use of an upgraded diffractometer X'Pert PRO PANalytical.

The Bragg – Brentano method with iron-filtered radiation of a cobalt lamp (CoKα) was used. Phase identification was done with the use of Philips X'Pert High Score software with the JCPDS database form 2001 (Fig. 3); the amount of austenite was determined experimentally.

Since no source data concerning transformations in the dual phase steels examined are available, transition temperatures Ac1, Ac3, Ms, Fs (see Table 3 [2, 7, 8]) and relative volume of the phases present in their microstructure were calculated from the formulae (1, 2, 3, 4).

Isothermal transformation diagrams (Fig. 4) were drawn from the formulae (1÷10,12) [1, 2, 7÷9]. Static tensile test was done with Instron 5585H machine (Table 2). Microhardness was measured with LECO LM700AT microhardness tester (Table 4).

Formulae (5÷14) necessary for drawing up the isothermal transformation diagram (Fig. 4) were presented by Victor Li M. [9].

Table 1. The chemical composition used in the studies of HCTxxxX dual-phase steel and Test x Rm samles determined spectrometrically

| Alloying elements | Chemical composition [%] | | | | | |
|---|---|---|---|---|---|---|
| | HCT 600X | HCT 780X | HCT 980X | Test 1 Rm | Test 2 Rm | Test 3 Rm |
| C | 0,082 | 0,143 | 0,156 | 0,13 | 0,15 | 0,086 |
| Si | 0,207 | 0,288 | 0,22 | 0,08 | 0,15 | 0,199 |
| Mn | 1,79 | 1,81 | 1,8 | 1,52 | 1,6 | 1,79 |
| Cu | 0,014 | 0,011 | 0,029 | 0,11 | 0,02 | 0,016 |
| V | 0,009 | 0,013 | 0,012 | 0,056 | 0,01 | 0,013 |
| Ti | 0,002 | 0,002 | 0,004 | 0,002 | 0,002 | 0,002 |
| W | 0,001 | 0,001 | 0,001 | 0 | 0,001 | 0,00 |
| Al | 0,035 | 0,037 | 0,029 | 0,002 | 0,02 | 0,034 |
| Mo | 0,001 | 0,008 | 0,176 | 0,005 | 0,15 | 0,001 |
| Ni | 0,013 | 0,016 | 0,02 | 0,14 | 0,02 | 0,014 |
| Cr | 0,366 | 0,430 | 0,411 | 0,450 | 0,42 | 0,391 |

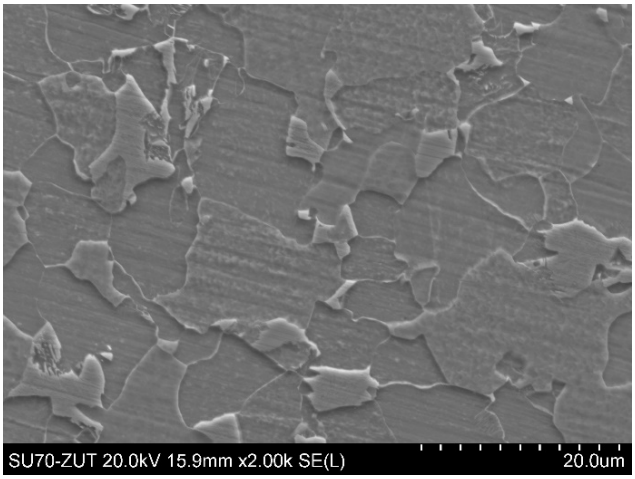


Fig. 2. Image of the microstructure of steel Test 2 Rm. The relative volume of ~ 58% of ferrite, martensite ~ 41%, 1% metastable residual austenite

Table 2. The mechanical properties of HCTxxxX dual-phase steel for cold forming acc. To EN 10346 [11] and examined Test x Rm sample.

| Steel name | Mechanical Properties, [MPa] | | | |
|---|---|---|---|---|
| | $R_e$ min | $R_e$ max | Rm min | Rm max |
| HCT600X | 340 | 420 | 600 | - |
| HCT780X | 450 | 560 | 780 | - |
| HCT980X | 600 | 750 | 980 | - |
| Test 1 Rm | 521 | - | 805 | 820 |
| Test 2 Rm | 653 | - | 1018 | 1020 |
| Test 3 Rm | 435 | - | 667 | 685 |

Table 3. Transition temperature and relative volume used in the studies of two-phase steel company SSAB and tested sample.

| Steel name | Temperature [C°] | | | | Relative volume [%] | | |
|---|---|---|---|---|---|---|---|
| | $F_s$ | $M_s$ | $Ac_1$ | $Ac_3$ | M | F | $A_{sz.}$ |
| HCT600X | 703 | 441 | 727 | 888 | 14 | 85 | 1 |
| HCT780X | 692 | 422 | 727 | 876 | 24 | 75 | 1 |
| HCT980X | 679 | 414 | 724 | 879 | 40 | 59 | 1 |
| Test 1 Rm | 722 | 434 | 721 | 869 | 16 | 83 | 1 |
| Test 2 Rm | 683 | 419 | 730 | 876 | 41 | 58 | 1 |
| Test 3 Rm | 701 | 441 | 731 | 885 | 17 | 82 | 1 |

- $F_s$ calculated from the formula Ferro P. [2]

(1) $Fs\ (^{o}C) = 870 - 270C - 80Mn\% - 70Cr\% - 83Mo\%$

- $M_s$ calculated from the formula Ferro P. [2]

(2) $Ms(C^{o}) = 539 - 423C - 30{,}4Mn\% - 17{,}7Ni\% - 12{,}1Cr\% - 7{,}5Mo\% + 10Co\% - 7{,}5Si\%$

- $Ac_3$ calculated from the formula Park S.H. [7]:

(3) $Ac3(^{o}C) = 955 - 350C\% - 25Mn\% + 51Si\% + 106Nb\% + 100Ti\% + 68Al\% - 11Cr\% - 33Ni\% - 16Cu\% + 67Mo\%$

- $Ac_1$ calculated from the formula Trzaska J. [8]:

(4) $Ac1(^{o}C) = 739 - 22{,}8C\% - 6{,}8Mn\% + 18{,}2Si\% + 11{,}7Cr\% - 15Ni\% - 6{,}4Mo\% - 5V\% - 28Cu\%$

Table 4 Microhardness of steel microstructures HV1

| Steel name | Hardness HV1 average | |
|---|---|---|
| | Ferrite | Martensite |
| HCT600X | 218 | 392 |
| HCT780X | 215 | 398 |
| HCT980X | 222 | 406 |

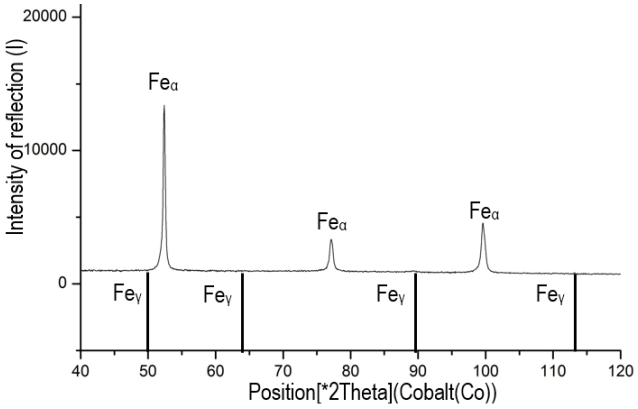


Fig. 3. X-ray diffraction HCT980X steel: delivered

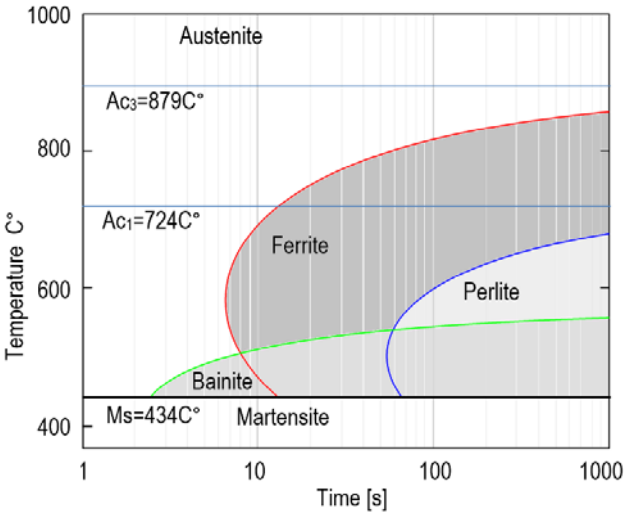


Fig. 4. Calculated HCT980X steel CCT diagram

The process of austenite grain nucleation and growth according to Avrami:

(5) $X = 1 - exp(-(k * s)^{a})$

X- function needed to transform part of volume B from part A, *k*- time constant, *s* –time, *a* i s- permanent characteristic of the kinetic transformation.

(6) $$S(X) = \int_0^X \frac{1}{X^{0,4(1-X)}(1-X)^{0,4X}} dX$$

A general model of the isothermal transformation diagram proposed by Kirkaldy:

(7) $$\tau(X,T) = \frac{F(C\%,Mn\%,Si\%,Ni\%,Cr\%,Mo\%,N\%)}{\Delta T^n \exp\left(-\frac{Q_{eff}}{RT}\right)} S(X)$$

where τ- time needed to transform a part of volume X from austenite, T- temperature, F- function dependent on alloy additions in steel, N- ASTM number, i.e. austenite grain size before the transformation, ΔT- super-cooling – temperature reduction, Qeff- efficient activation energy for the diffusion n= degree of freedom, S(X) – reaction time index defined by the approximation of phase transformations, R- gas constant.

(8) $$\tau_F = \frac{PF}{2^{0,41N}\left(Ae_3 - T\right)^3 \exp\left(-\frac{27500}{RT}\right)} S(X)$$

(9) $$\mathrm{PF} = \exp(1 + 6{,}31C\% + 1{,}78Mn\% + 0{,}31Si\% + 1{,}12Ni\% + 2{,}7Cr\% + 4{,}06Mo\%)$$

(10) $$\tau_P = \frac{PP}{2^{0,32N}\left(Ae_1 - T\right)^3 \exp\left(-\frac{27500}{RT}\right)} S(X)$$

(11) $$\mathrm{PP} = \exp\left(-4{,}25 + 4{,}12C\% + 4{,}36Mn\% + 0{,}44Si\% + 1{,}71Ni\% + 3{,}33Cr\% + 5{,}19\sqrt{Mo\%}\right)$$

(12) $$\tau_B = \frac{PB}{2^{0,29N}\left(Bs_3 - T\right)^2 \exp\left(-\frac{27500}{RT}\right)} S(X)$$

(13) $$\mathrm{PB} = \exp(-10{,}23 + 10{,}18C\% + 0{,}85Mn\% + 0{,}55Ni\% + 0{,}9Cr\% + 0{,}36Mo\%)$$

(14) $$Bs = 637 - 58C\% - 35Mn\% - 15Ni\% - 34Cr\% - 41Mo\%$$

**Modelling conditions and results**

Material database containing around 60 records of different dual-phase steels was created. The records included data concerning the chemical composition of steels, their $Ac_1$ and $Ac_3$, $F_s$ and $M_s$, Re and Rm transition temperatures as well as the relative volume of the phases in the microstructure.

In order to calculate the minimal tensile strength and yield strength of dual phase steels, the data were modelled using artificial neural networks (see Fig. 5).

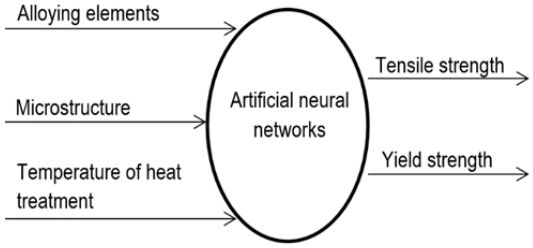


Fig. 5 Schematic model of artificial neural network is used to determine the mechanical properties.

The model defines the following relationships: steel chemical composition→ isothermal transformation diagram CCT→ heat treatment→ microstructure (volume of fraction)→ steel mechanical properties. The modelling consisted process was divided into the following stages:

I. data collection
II. neural network training and learning
III. trained neural networks testing
IV. validation of the network
V. the network selection of the best qualitative properties for advance modelling.

In order to design the chemical composition of dual-phase steels that would have the required tensile strength, the BFGS (Broyden-Fletcher-Goldfarb-Shanno) training algorithm was used. MLP 9-11-2 multilayer feedforward neural network (9 inputs, 11 neurons in the hidden layer, 2 outputs: Re- yield strength and Rm- tensile strength) with the logistic activation function was used for prediction.

The number of neurons in the hidden layer was selected experimentally. The network generates two output signals. The properties of the neural network can be found in Table 6. The figure 6 shows the correlation between the input and output data after artificial net validation. Validating the data are subject to tensile strength.

Simulation of network shows the influence of two selected sample alloying elements, such as carbon, silicon, chrome and manganese, on tensile strength of steel with fixed heat treatment conditions and constant concentration of the rest of the elements. Figures 7÷9 feature the results of the simulation for different elements.

Table 5. Accepted to simulate the influence of two alloying elements and temperature transformation Ac3 and Ac1

| Content | Alloying elements | | | | Transformation temp. [C°] | |
|---|---|---|---|---|---|---|
| | C% | Si% | Mn% | Cr% | $Ac_1$ | $Ac_3$ |
| min. | 0,05 | 0,05 | 1,5 | 0,1 | 710 | 860 |
| maks. | 0,2 | 0,3 | 1,9 | 0,5 | 740 | 920 |

Table 6. Details of the selected neural network

| Id network | Network name | Quality (learning) | Error (learning) |
|---|---|---|---|
| 3 | MLP 9-11-2 | 0,9997 | 5,8624 |
| The error | Learning algorithm | Quality (test) | Error (test) |
| SOS | BFGS 68 | 0,9989 | 40,2578 |
| Activation (hidden layer) | Activation (output) | Quality (validation) | Error (validation) |
| logistics | linear | 0,9913 | 91,7992 |

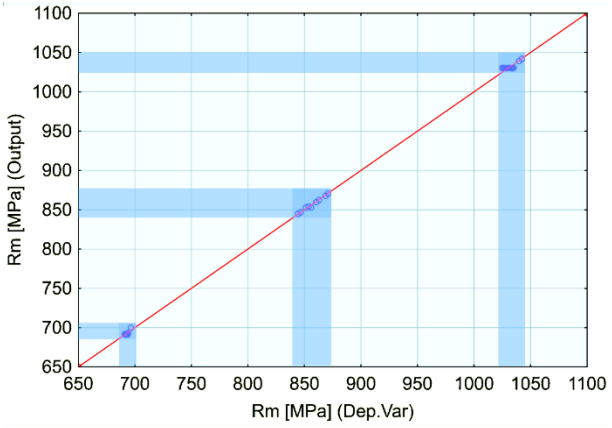


Figure 6 Correlation of results generated by modeling the neural network MLP 9-11-2 (Dep. Var) with experimental results (output)

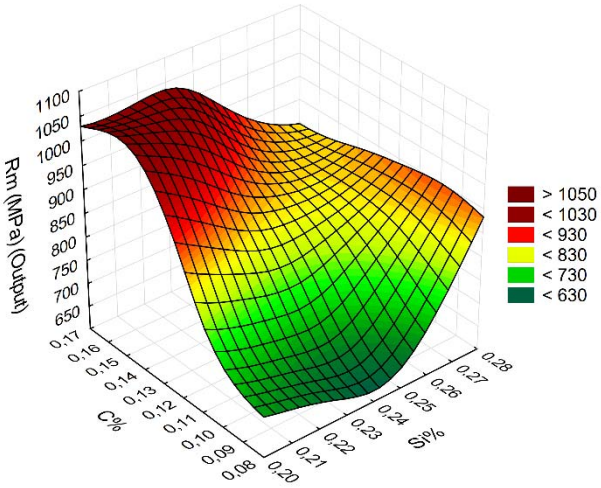


Fig. 7. Effect of the concentration of carbon and silicon on the tensile strength of dual phase steels

The artificial neural network is to forecast the mechanical properties of the steels according to a given chemical composition, the conditions of heat treatment and the relative volume of the phase in the microstructure.

Neural network training, learning, test and validation data were randomly selected from the material database. Both the microstructure and the influence of the chemical composition on the temperatures of Ac1, Ac3, Fs, Ms transitions are worked out for the sake of simulating the relations between heat treatment and the relative volume of a given phase in the microstructure of the steel.

The scope of the concentration of the elements was selected for the simulation and forecast (Table 5 features only the most important elements).

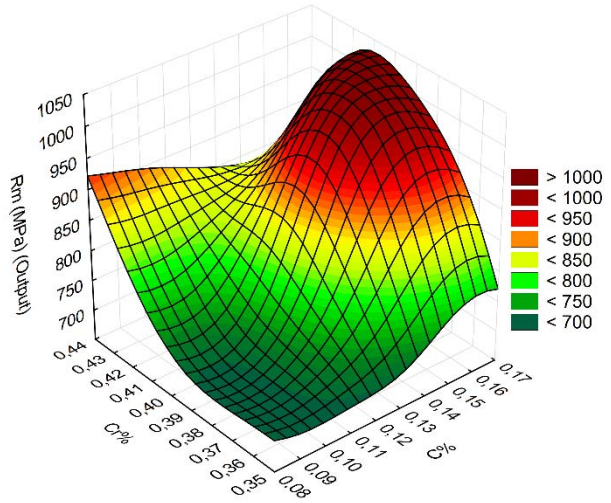


Fig. 8. Effect of the concentration of chrome and carbon on the tensile strength of dual phase steels

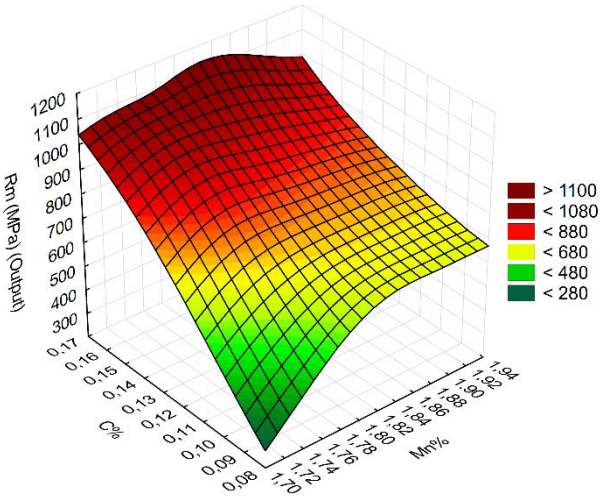


Fig. 9. Effect of the concentration of manganese and carbon on the tensile strength of dual phase steels

## Conclusion

Proposed method of calculation the minimum tensile strength and yield strength dual phase steels using the artificial neural networks is a first step in modelling relationship of chemical composition and properties, and consider the successive DP steels based on a database including existing examination results.

In the model elaborated for the purpose of database records containing 60 used: the temperature transformation steel, chemical composition and the relative volumes of the phases in the microstructure as a function of chemical composition and heat treatment parameters.

The model allows estimating influence of these factors, particularly chemical composition on mechanical properties of dual-phase steels and the results obtained prove the relevance of neural networks. Prediction of the properties samples the examined Test 1 Rm – Test 3 Rm test confirms the validity of the model (with a tolerance of ~4%).

Tensile strength Test 1 Rm samples was determined experimentally $Rm_{min}$ - $Rm_{max}$ 805 ÷ 820 MPa-, MLP neural network prediction of 9-11-2 gave results ~ 825MPa.

Tensile strength Test 2 Rm samples was determined experimentally $Rm_{min}$ - $Rm_{max}$ 1018 ÷ 1020 MPa, MLP neural network prediction of 9-11-2 gave results ~ 998 MPa.

Tensile strength Test 3 Rm samples was determined experimentally $Rm_{min}$ - $Rm_{max}$ 667 ÷ 685 MPa-, MLP neural network prediction of 9-11-2 gave results ~ 642 MPa.

The results of prediction neural network confirm previous authors investigation results in the works [12, 13].

***Authors**: Sławomir Krajewski, West Pomeranian University of Technology, Szczecin, Institute of Materials Science and Engineering, Al. Piastow 19 St., 70 - 310 Szczecin, Poland, e-mail: skrajewski@zut.edu.pl*

*Jerzy Nowacki, West Pomeranian University of Technology, Szczecin, Institute of Materials Science and Engineering, Al. Piastow 19 St., 70 - 310 Szczecin, Poland, e-mail: jerzy.nowacki@zut.edu.pl*

REFERENCES

[1]. Gür C. H., Pan J.: Thermal Process Modeling of Steels, *Taylor & Francis Group* 2009.

[2]. Ferro P.: The Use of Matlab in Advanced Design of Bonded and Welded Joints, *Applications of MATLAB in Science and Engineering*, 09/2011 ISBN 978-953-307-708-6 2010, 387-408.

[3]. Guo-hui ZHU, Xue-hui ZHANG, Wei-min MAO: Development in high-grade dual phase steels with low C and Si design, *Front. Mater. Sci. China* 2009, 3(4): 442–446.

[4]. Hofmann H., Mattissen D., Schaumann T. W.: Advanced cold rolled steels for automotive applications, *Steel Research International Issue* 1/2009 717.

[5]. Lis A.K., Gajda B.: Modeling of the DP and TRIP microstructure in the CMnAlSi automotive steel, *Journal of Achievements in Materials and Manufacturing Engineering*, Volume 15 Issue 1-2, 2006.

[6]. Miernik K., Bogucki R., Pytel S.: Wpływ temperatury hartowania na mikrostrukturę i własności mechaniczne stali Dp, *Czasopismo Techniczne- Mechanika*, Wydawnictwo Politechniki Krakowskiej 2-M/2009 Zeszyt 6 Rok 106.

[7]. Park, S.H.: Development of Ductile Ultra-High Strength Hot Rolled Steels, *Posco Technical Report*, 1996, 50-128.

[8]. Trzaska J.: Modelling of CCT Diagrams for Engineering and Constructional Steels, *Journal of Materials Processing Technology*, 192-193, 2007, 504-510.

[9]. Victor Li M., Niebuhr V. D., Meekisho, L. L., Atteridge, G. D.: A Computational Model for the Prediction of Steel Hardenability, *Metallurgical and Materials Transactions*, 1998 B, Vol. 29B, pp. 661-672.

[10]. Yi H. L., Lee K. Y., Bhadeshi H. K. D. H.: Stabilisation of ferrite in hot rolled δ- TRIP steel, *Materials Science and Technology* Vol. 27 No 2/2011 528.

[11]. EN 10346 Continuously hot-dip coated steel flat products for cold forming. Technical delivery conditions

[12]. Krajewski S., Nowacki J., Modelowanie właściwości dwufazowych stali DP z zastosowaniem sztucznej inteligencji, *Inżynieria Materiałowa* 6 (2012) 372 – 376

[13]. Krajewski S., Nowacki J., Dual-phase steels microstructure and properties consideration based on artificial intelligence techniques *Archives of Civil and Mechanical Engineering* Vol. 14 No 2 (2014) 278-286